THE ASTROPHYSICAL JOURNAL, 462:326–338, 1996 May 1

RADIO RECOMBINATION LINES FROM INNER GALAXY DIFFUSE GAS. I. HIGH-SENSITIVITY OBSERVATIONS: He^+/H^+ AND CARBON

CARL HEILES,[1] BON-CHUL KOO,[2] N. A. LEVENSON,[1] AND WILLIAM T. REACH[3]
Received 1995 May 19; accepted 1995 September 21

ABSTRACT

We have observed radio recombination lines (RRLs) at $\sim$1.4 GHz toward the Galactic interior at hundreds of positions in a separately published survey. In some cases we observe not only the Hα but also the Hγ, Hδ, Heα, and Cα RRLs. We use previously published theory to estimate the enhancement in line intensity from non-LTE excitation, which amounts to $\sim$30% for all of the α lines; however, the theory does not agree with our observed ratios of α to higher order line intensities. Intensity ratios of α lines of different elements should be unaffected by non-LTE excitation.

The ratio $(n_{He^+}/n_{He})/(n_{H^+}/n_H) \lesssim 0.13$ in the diffuse ionized medium of the Galactic interior. This is difficult to explain, because photons with energy greater than 24.6 eV must be systematically excluded from this gas. If O stars are the source of the ionizing photons, then this implies an upper mass limit on the initial mass function. However, with this upper mass limit, stars cannot produce enough ionizing photons to satisfy the total Galactic ionization requirement. One solution to this quandary is to invoke larger uncertainties in various processes than we estimate. Other solutions require an ionization source other than stars as currently understood, and we discuss two possibilities.

We detect the C RRL toward several H II regions. The C RRLs are too strong to come from H ionized gas and must come instead from photodissociation regions. We compare the C RRL with the C^+ 158 μm line toward W43 and derive relatively unambiguous values for physical parameters in the associated photodissociation region.

Subject headings: H II regions — ISM: abundances — radio lines: ISM

1. INTRODUCTION

The warm ionized medium (WIM) is one of the four major components of the diffuse interstellar medium (Kulkarni & Heiles 1987). It amounts to $\sim$25% of the H I mass in the solar neighborhood. In the Galactic interior,[4] it becomes a much larger fraction of the H I mass and $\langle n_e^2 \rangle$ becomes large enough for it to become observable as the emitter of "diffuse radio recombination lines" (diffuse RRLs) at radio frequencies of $\sim$1.4 GHz. The WIM in the Galactic interior was first considered by Mezger (1978), who called it the "extended low-density ionized" (ELD) gas. Here, following Petuchowski & Bennett (1993) and Heiles (1994), we refer to this gas as ELDWIM.

The physical properties of the local WIM are reviewed and considered theoretically by Mathis (1986) and Domgörgen & Mathis (1994). The observed optical line ratios of the local WIM are well matched if the ionization is produced by a weak ultraviolet radiation field whose spectral distribution comes from an initial mass function–compatible weighted mean of O5–O9.5 stars. In particular, their theory predicts $(n_{He^+}/n_{He})/(n_{H^+}/n_H) \equiv \chi_{He}/\chi_H = 0.4$–$0.6$. Optical observations of this ratio in the local WIM have been made by Reynolds & Tufte (1995), who find the upper limit $\chi_{He}/\chi_H \lesssim 0.27$. This low value poses severe difficulties for models in which the WIM is ionized by O star photons, because the temperature of the representative star must be $\lesssim$36,000 K. Galaxy-wide, if the WIM is to be ionized only by such stars, then the required initial mass function (IMF) has a disturbingly small upper mass limit (see § 5.2 below).

For several years we have been engaged in a survey of the inner Galaxy RRL emission from the ELDWIM at several hundred positions. The primary aim of this survey was to map the RRL emission from "worm" structures (Koo, Heiles, & Reach 1992; Heiles, Reach, & Koo 1995, hereafter HRK). The present paper discusses the secondary goal, which was to determine the χ_{He}/χ_H ratio. We have determined this ratio observationally in two ways. In one we achieve long effective integration times by averaging observations at many positions. In the other we observe specific positions for long times. As in the solar vicinity, we find low ratios χ_{He}/χ_H, ranging from values somewhat higher than the upper limit of Reynolds & Tufte (1995) to much smaller.

In addition, we find detectable C RRLs toward giant H II regions and other regions where the H RRL is intense. These are reminiscent of such lines detected in the early 1970s by pioneers of RRL observations, and the interpretation now is the same as then, namely, that the C RRLs come from cold, dense photodissociation regions (PDRs).

We discuss the observations in § 2, the He RRL results in § 3, and the C RRL results in § 4.5. Section 5 considers several explanations for the He results. One provides a severe constraint on the upper mass limit of the IMF that is incompatible with the Galaxy-wide ionization requirement. Another mentions the recent discovery (Cassinelli et al. 1995) that B stars produce enhanced output of ionizing photons over that theoretically predicted. The third considers Sciama's (1990) hypothesis that the WIM is ionized by photons from the decay of dark matter and concludes that the production rate of such photons is inadequate to

[1] Astronomy Department, University of California, Berkeley, CA 94720; cheiles@astro.berkeley.edu, nlevenson@astro.berkeley.edu.
[2] Seoul National University, Astronomy Department, Seoul 151-742, Korea; koo@astrohi.snu.ac.kr.
[3] Universities Space Research Association, NASA/Goddard Space Flight Center, Code 685, Greenbelt, MD 20771; reach@stars.gsfc.nasa.gov.
[4] Here the term "Galactic interior" connotes the region of the Galaxy where the RRLs are prominent, which is mostly 4 kpc $\lesssim R_{gal} \lesssim$ 7 kpc, where R_{gal} is the Galactocentric radius (Heiles, Reach, & Koo 1995).

produce the observed ratio continuum and RRL emission from the inner Galaxy.

2. OBSERVATIONS

2.1. *Data from Hat Creek Radio Observatory (HCRO)*

Some years ago we began the RRL survey with the 85 foot (26 m) telescope of HCRO.[5] This telescope had HPBW = 36′ and was equipped with two ~40 K receivers in orthogonal circular polarizations and a 1024 channel spectral autocorrelator; details are in Heiles (1989). We observed RRLs at two frequencies and in two polarizations simultaneously. All observations herein used the 165α and 167α RRLs, which are centered near 1451 and 1400 MHz, respectively; these RRLs were selected because they were quite clear of interference. We observed a bandwidth of 5.0 MHz and frequency-switched by 2.5 MHz, keeping the lines "within the band." With this arrangement, our total useful bandwidth is 2.5 MHz, which is about 4.5 times larger than the separation between the He and H RRLs, and the frequency resolution is 23.6 kHz (1.21 times larger than the channel separation; Cooper 1976), which is equivalent to about 5.0 km s^{-1}.

We restricted our survey to positions having $|b| \geq 0.^\circ 6$, because $b = 0^\circ$ had already been surveyed by Lockman (1976, 1980) and Cersosimo (1990a, b). We detected the H RRL at many positions, most having a signal-to-noise ratio (S/N) insufficient to detect the He RRL. To increase the effective integration time, we averaged the data at different positions. We "lined up" spectra by centering the detected H RRL for each spectrum at the center of the average spectrum; because all of the lines are centered at different velocities, the average spectrum does not have a meaningful velocity zero point. We weighted each contribution to the average by the square of its S/N in the H RRL.

We selected data for a few chosen ranges of position and intensity. Some of these averages include a small number of positions that have fairly strong RRLs, which usually lie near strong H II regions, and some include many positions that have weaker RRLs.

One is the Stockert Chimney (Müller, Reif, & Reich 1987), which we denote by the term "S54 worm–S54;" this worm contains the powerful H II region S54. This average includes all 11 of our positions lying between $l = 17^\circ$ and 21°, $b = 1^\circ$ and 6°, except for one position $[(l, b) = (18.^\circ 6, 1.^\circ 8)]$ lying on S54 itself.

Our average for the "W43 worm base" includes only two positions, G30.25−0.50 and G31.25−0.5, which have H RRL intensities of about 185 and 100 mK, respectively. These positions are not only quite intense but also lie at the base of this worm and, as such, are not representative of the worm itself. For this average alone, the data have been Hanning smoothed in the plot. The intensities for other positions in this worm are much smaller, and their H RRLs have a broad second velocity component displaced toward the He RRL; this combination of circumstances makes these positions not useful for our purposes.

Our average for "$T_A > 100$" included all 13 positions in our survey for which the peak antenna temperature of the H RRL exceeds 100 mK; T_A ranges from 102 to 206 mK. Despite the factor of 2 in intensity, no individual spectrum dominated the average. These positions usually lie close to giant H II regions and include the following: G0.00−0.60, G0.00+0.60, G0.60+0.60, G0.60−0.60, G15.00−1.20 ($0.^\circ 5$ from M17), G16.80+0.60 ($0.^\circ 3$ from M16), G17.06+1.28 ($0.^\circ 4$ from M16), G17.40+0.60 ($0.^\circ 5$ from M16), G18.60+1.80 (the H II region S54), G18.60+2.40 ($0.^\circ 4$ from S54), G30.60−0.60 ($0.^\circ 6$ from W43), G49.20−0.60 ($0.^\circ 3$ from W51), and G84.60−0.60 ($0.^\circ 3$ from G84.8−0.4; Reifenstein et al. 1970).

Our average for "$T_A < 100$" included all 138 positions in our survey for which the peak antenna temperature of the H RRL is less than 100 mK. Most positions lie in the longitude range 0°–41°; also, there are nine in the longitude range 77°–86° and nine in the longitude range 151°–202°.

Figure 1 presents the spectra for these averages. We provide fiducial marks for the He and C RRLs that would be centered at the same velocity as the H RRL. Table 1 presents the results of Gaussian fitting.

2.2. *Data from National Radio Astronomy Observatory (NRAO)*[6]

Based on the HCRO survey, we selected several fairly intense positions for deep integration with the 140 foot (43 m) telescope of NRAO. This telescope has HPBW = 21′ and was equipped with two ~20 K receivers in orthogonal linear polarizations and a 1024 channel spectral autocorrelator; the autocorrelator specifications were the same as those at Hat Creek, and we used the identical observing technique. System temperatures on the sky for our positions were raised to above 30 K by the Galactic continuum radiation and ground pickup, to above 40 K for S54 and G30.25−0.50, and to much higher for the H II regions W43 and M17. We used different RRL transitions, depending on the interference environment; these included H165α (~1450 MHz), H168α (~1375 MHz), and H169α (~1350 MHz). We also tried the H166α line (~1425 MHz) but found the data to be unusable because of leakage of the much stronger 21 cm line into the image of the baseband mixer.

We obtained useful spectra for six positions. Figure 2 presents the spectra and Table 1 the Gaussian fits. Except for well-known H II regions, the positions are referred to as GLL.LL ± BB.BB, where LL.LL and BB.BB are the Galactic coordinates in decimal degrees. For the H II regions, the Galactic coordinates are as follows: M17 = G15.05−0.68; W43 = G30.76−0.03, and S54 = the average of G18.60+1.80 and G18.47+1.93. The spectrum for G18.25+2.70 contained two strong interference spikes, one in channels −18 to −23 and one in channel −37; these were set to zero in Figure 2*b* for the sake of clarity.

In Figure 2 we provide fiducial marks as in Figure 1, together with two other fiducial marks: one for H243γ (which happens to lie 0.57 MHz below the H169α line), and one for $He^+267\alpha$ (0.19 MHz above the H168α line). The intensities of these lines as shown on Figure 2 are reduced from their true intensities because each spectrum on Figure 2 is the average of Hα RRL spectra for at least two different frequencies, while the H243γ and $He^+267\alpha$ lines appear at only one frequency. We discuss the H243γ line below in § 3.1.2.

2.3. *Gaussian Fits and Estimates of Integrated Line Intensity*

Table 1 provides Gaussian fit parameters for the H RRLs and, when they were detected, for the He and C RRLs.

[5] This telescope was destroyed by a windstorm on 1993 January 21.

[6] The NRAO is operated by Associated Universities, Inc., under contract with the National Science Foundation.

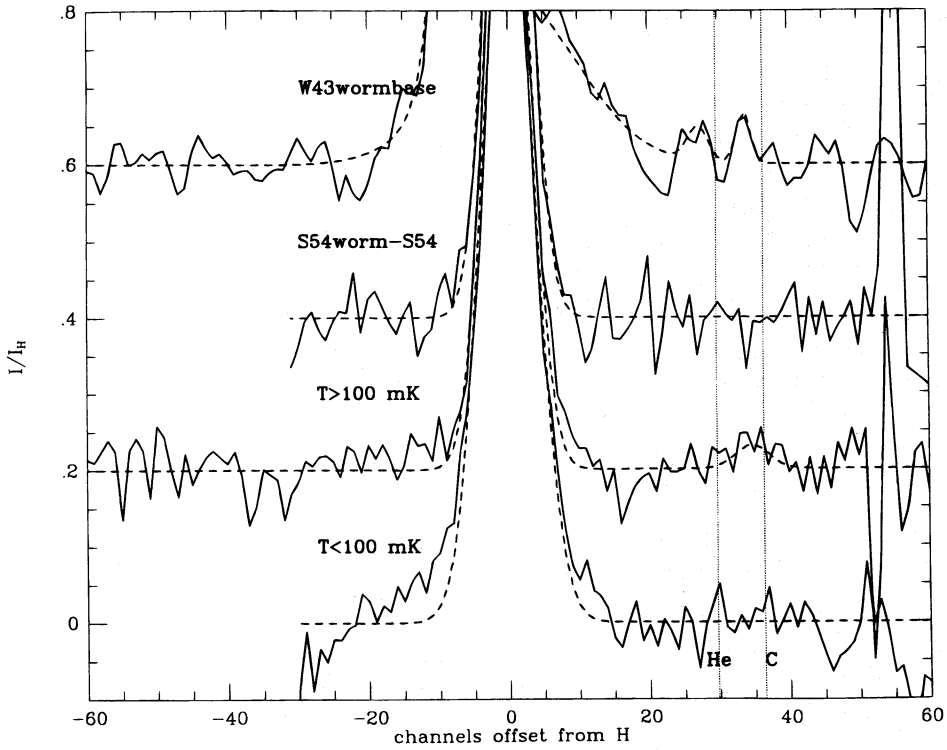

FIG. 1.—Four averages of RRLs for HCRO data. Each spectrum is the average of many positions, and also of 165α and 167α lines, as described in § 2.1. For each spectrum, the intensity scale is in units of the intensity of the Gaussian fit to the H RRL as given in Table 1. The solid lines are the data. The dashed lines are the Gaussian fits to the spectra, which are summarized in Table 1. The vertical dotted lines are fiducial marks for the He and C RRLs that would correspond to the H RRL if they had the same velocity.

Some of the spectra have two H velocity components as noted. Tables 2 and 3 provide the ratios of integrated line intensities and their uncertainties, derived as explained below. All uncertainties are 1 σ.

To estimate a C or He line integral when the line is strong enough to be fitted by a Gaussian, we take the product of the derived Gaussian intensity and width. We calculate the uncertainty in the integral by propagating the uncertainties in the intensity and width in the standard manner.

To estimate the ratio of a C or He line integral to the H line integral when the line is not strong enough to be fitted by a Gaussian, we sum the spectrum for the H and C or He lines over the center channel ± half the H-line FWHM in channels. The center channel for the H RRL is that derived from the Gaussian fit, and that for C or He is displaced by the predicted offset for the line. The errors on these sums are taken to be the channel-to-channel rms noise multiplied by the square root of the number of channels included in the sum. With our use of half the FWHM, the channel ranges for the C and He lines do not overlap.

Some of our spectra include two other lines, H242γ (§ 3.1.2 below) and $He^+267\alpha$. The latter line appears to have been detected for W43 and G30.25−0.50, but these are simply additional velocity components because they also appear in the spectra of H RRLs at other frequencies, which do not have a $He^+\alpha$ line in close proximity. Just as a check,

TABLE 1

GAUSSIAN FITS FOR H, He, AND C RRLs[a]

Name	v(H) (km s^{-1})	T_A(H) (mK)	dv(H)[b] (km s^{-1})	T_A(He) (mK)	dv(He)[b] (km s^{-1})	cc(He)[c] (channels)	T_A(C) (mK)	dv(C)[b] (km s^{-1})	cc(C) (channels)
W43 worm base.....	...	125.5(2.9)	31.1(0.5)	5.7(2.7)	13.9(4.5)	32.1(0.8)	8.7(3.2)	9.4(4.5)	38.6(0.4)
S54 worm–S54	...	86.9(1.5)	27.2(0.3)	...	...	...	...	...	...
$T_A > 100$	...	166.1(2.6)	29.1(0.3)	...	...	...	5.2(2.9)	22.9(9.1)	34.8(1.5)
$T_A < 100$	...	50.9(0.9)	35.2(0.5)	...	...	...	...	...	...
S54	30.5	323.3(4.0)	27.0(0.20)	23.9(4.7)	19.5(2.9)	28.4(0.4)	6.8(6.0)	11.8(7.6)	34.7(1.2)
W43	95.6	587.0(5.2)	36.6(0.3)	21.0(7.2)	18.0(4.7)	28.9(0.7)	38.9(7.1)	18.8(2.6)	35.9(0.4)
M17	18.5	1497.0(14.0)	42.2(0.3)	134.7(18.5)	25.5(3.2)	28.7(0.5)	194.4(21.9)	17.1(1.6)	35.7(0.3)
G18.25+2.70	26.9	52.6(1.2)	24.3(0.4)	2.2(1.2)	25.4(9.8)	29.8(1.5)	...	...	...
G18.60+2.40	27.9	101.3(1.1)	27.7(0.2)	4.9(1.3)	17.2(3.3)	27.1(0.5)	...	...	...
G30.25−0.50	101.2	123.2(2.4)	24.6(0.3)	6.1(2.1)	12.9(3.2)	29.0(0.5)	8.4(1.9)	15.6(2.6)	35.2(0.4)

NOTES.—The following positions have a second H RRL component: W43 worm base: $T_A = 16.3$, $dv = 89.4$, cc = 6.0; S54: $T_A = 8.7$, $dv = 12.2$, cc = 17.1; W43: $T_A = 97.0$, $dv = 26.5$, cc = 11.7; G30.25−0.50: = 32.0, $dv = 69.4$, cc = 4.9.

[a] Each fitted RRL is the average of two or more α lines (see § 2). Numbers in parentheses are the 1 σ uncertainties.

[b] dv is the FWHM in km s^{-1}.

[c] cc is the center channel relative to the H RRL. See text for expected values. We do not regard the He and C fits for the first three spectra as real detections (see § 2.3).

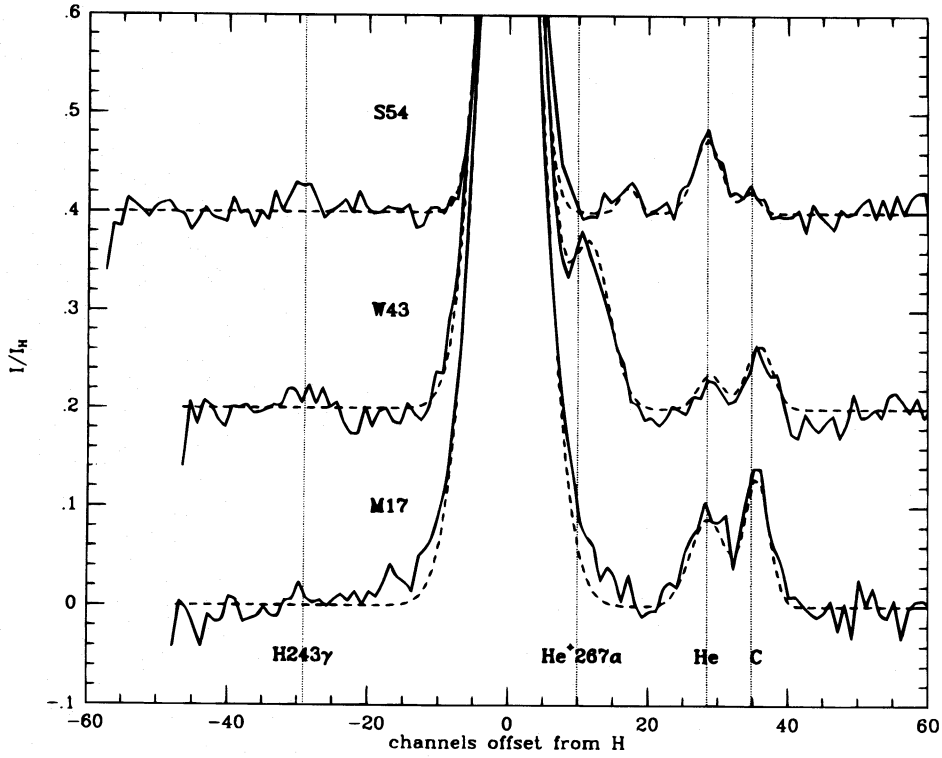

FIG. 2*a*

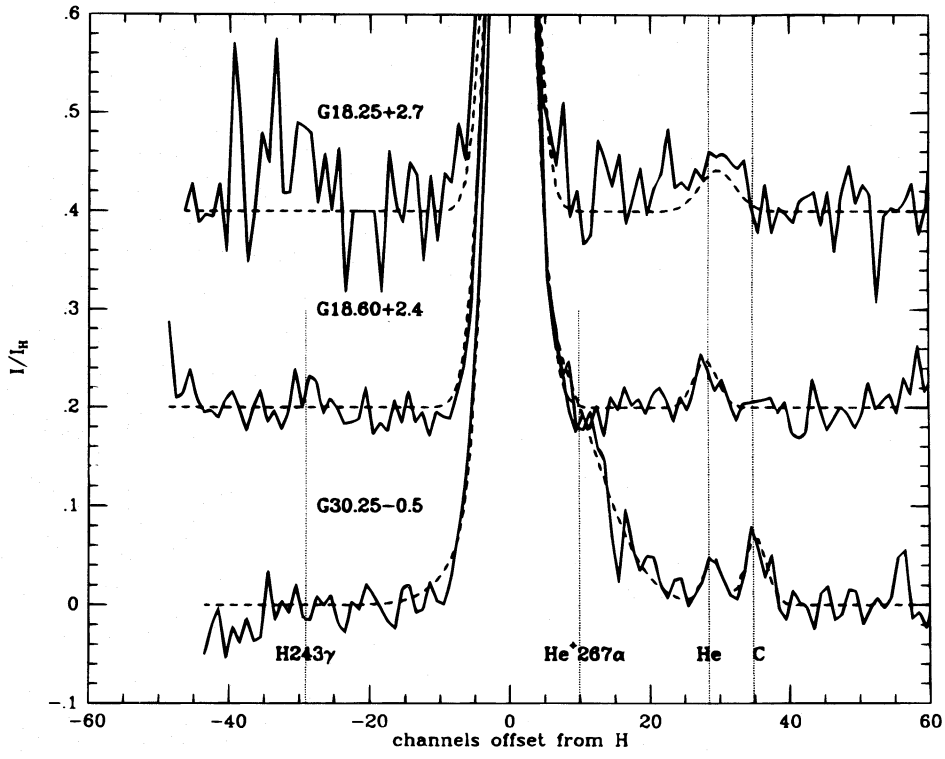

FIG. 2*b*

FIG. 2.—RRLs for NRAO data. Each spectrum is the average of at least two α lines, as described in § 2.2. For each spectrum, the intensity scale is in units of the intensity of the Gaussian fit to the H RRL as given in Table 1. The solid lines are the data. The dashed lines are the Gaussian fits to the spectra, which are summarized in Table 1. The vertical dotted lines are fiducial marks for the He and C RRLs that would correspond to the H RRL if they had the same velocity, and for the H243γ and $He^+267\alpha$ RRLs where appropriate; the latter lines occur with reduced intensities (see text). The H243γ line is correctly shown in Fig. 3. Fig. 2*a* presents data for well-known H II regions and Fig. 2*b* for positions that do not fall on well-known H II regions.

we observed a few suspect positions in the $He^+268\alpha$ and $He^+269\alpha$ and achieved no detections. We will find below that He^+ is underabundant relative to theoretical models; the absence of detectable $He^+\alpha$ shows that the remaining He is neutral, not He^{++}. The transition probability for α recombination lines at a given frequency depends only on Z^2, where Z is the charge of the nucleus; thus each He^{++} ion contributes intrinsically 4 times more to the $He^+\alpha$ RRL

TABLE 2

RATIOS OF H243γ/H169α AND H267δ/H169α

Name	H243γ/H169α	H267δ/H169α
W43	0.051(0.013)	...
S54	0.145(0.063)	...
G18.60+2.40	0.107(0.031)	...
G30.25−0.50	0.074(0.011)	0.052(0.010)
Theoretical[a]	0.128	0.073

[a] Theoretical ratios assuming LTE (Menzel 1968).

than each He^+ ion does to the Heα RRL. Thus the absence of detectable $He^+\alpha$ RRLs effectively rules out the possibility that significant He^{++} exists in the ELDWIM—a result that is hardly surprising.

For the HCRO spectra in Figure 1, the He and C RRLs should be displaced from the H RRL by 29.8 and 36.4 channels, respectively. Table 1 lists only one HCRO spectrum, W43 worm base, as having a possible He RRL detection. However, it does not have the appropriate central channel, nor does the "detection" look reliable (in our opinion). Table 1 lists two HCRO spectra as having possible C RRL detections. Neither of the C RRLs has the appropriate displacement, and furthermore, the "detection" for the $T_A >$ 100 position is very wide, which makes it intrinsically suspicious. We regard none of these He and C RRL "detections" as real.

For the NRAO spectra in Figure 2, the He and C RRLs should be displaced from the H RRL by 28.4 and 34.8 channels, respectively. Table 1 lists all NRAO spectra as having He RRL detections and all but two as having C RRL detections. All of these detections have the appropriate central channels and look reasonable, with the possible exception of the He RRL for G18.25+2.7. We accept all of these as real detections.

3. He AND H RRLs

3.1. *Radiative Transfer Considerations*

3.1.1. *Theoretical Estimates*

First, we consider whether non-LTE effects are signficant for these RRLs. We note that most discussions (e.g., Walmsley 1980) are oriented toward H II regions, for which the radio continuum comes primarily from the H II region itself; these do not apply for our case, for which most of the continuum comes from unrelated background regions and makes stimulated emission more important. The integrated RRL intensity from element "X" is[7]

$$\int T_{B,X}\,dv = f_{\rm NLTE}\,6.2\times10^{-4}\nu_9^{-1}T_4^{-3/2}n_e\,n_{X^+}\,L_{\rm pc}\ {\rm K\ km\ s^{-1}}\,, \tag{1}$$

where the symbols have their usual meanings, the volume densities are in cm^{-3}, T_4 is the temperature in units of 10^4 K, ν_9 is the line frequency in GHz, and $f_{\rm NLTE}$ accounts for non-LTE effects and is equal to unity plus the ratio of stimulated to spontaneous emission; $f_{\rm NLTE} = 1$ for the LTE case. For a weak ionized region (upon which is incident a continuum brightness temperature T_B from behind) or a strong region (for which T_B also includes an appropriately weighted contribution from the H II region itself, which is equal to half the continuum temperature generated within the H II region) and under the assumptions $T_e \gtrsim 1000$ K and $T_B/T_e \ll 1$, it is easy to show that

$$f_{\rm NLTE} = b_n\left(1 + \frac{k}{h\nu}\,\Delta n\,\frac{d\ln b_n}{dn}\right), \tag{2}$$

where the symbols have their usual meanings, b_n is the departure coefficient from LTE, and Δn is the order of the transition (an α transition has $\Delta n = 1$) (Goldberg 1966); for our RRLs, $h\nu/k = 0.068$ K.

For our positions that are not associated with H II regions, HRK show that the electron density in the emitting regions $n_e \sim 5\ cm^{-3}$ at $z = 0$, with probable smaller values at higher z. This range is consistent with the somewhat larger range $5 < n_e < 22\ cm^{-3}$ estimated by Müller et al. (1987) for the S54 worm; their larger values lie in the more intense portion of the worm where $T_{B,H} \gtrsim 100$ mK, which is a high intensity in our RRL survey. Classical calculations of b_n do not extend to densities as low as $n_e = 1\ cm^{-3}$, so we judiciously extrapolate from Brocklehurst's (1970) results, which extend down to $n_e = 10\ cm^{-3}$, using the convenient graphical presentation of Sejnowski & Hjellming (1969) as a guide. HRK find $T_e \sim 7000$ K for the ELDWIM; here we consider the nearest value in the theoretical tables, which is $T_e = 5000$ K. For $n_e = 10\ cm^{-3}$ and $n = 170$, Brocklehurst finds $b_n = 0.95$ and $(d\ln b_n)/dn = 1.4\times10^{-3}$. Because of inflections in the curves, $(d\ln b_n)/dn$ appears to remain roughly independent of n_e near $n = 170$, so for $n = 170$, a reasonable extrapolation to $n_e = 1\ cm^{-3}$ appears to be $b_n \sim 0.8$ and $(d\ln b_n)/dn \sim 1.4\times10^{-3}$. If this is correct, then there is no significant dependence of $f_{\rm NLTE}$ upon n_e in this range and for the Hα lines we adopt $b_n = 0.9$ and $(d\ln b_n)/dn = 1.4\times10^{-3}$. For use below in our discussion of the H243γ line, we perform the same exercise and obtain $b_{240} \approx 1$, and $(d\ln b_n)/dn \sim 2.26\times10^{-4}$ and 1.27×10^{-3} for $n_e = 10$ and $1\ cm^{-3}$, respectively; the results do depend significantly on n_e through the stimulated emission term $(d\ln b_n)/dn$.

The above give the following: For Hα with $n \sim 167$, we have $f_{\rm NLTE} \sim 0.9(1 + 0.021T_B)$. For H243γ with $n_e = 10\ cm^{-3}$, we have $f_{\rm NLTE} \sim 1 + 0.010T_B$. For H243γ with $n_e = 1\ cm^{-3}$, we have $f_{\rm NLTE} \sim 1 + 0.056T_B$.

Toward the Galactic interior, most of the radio continuum intensity at 1.4 GHz is synchrotron radiation,

TABLE 3

RATIOS OF He/H AND C/H INTEGRATED RRL INTENSITIES

Name	He/H	C/H
S54 worm–S54	−0.004(0.013)	−0.010(0.013)
W43 worm base	0.020(0.012)	0.021(0.013)
$T_A > 100$	0.016(0.010)	0.025(0.017)
$T_A < 100$	−0.000(0.011)	0.012(0.011)
S54	0.053(0.013)	0.009(0.010)
W43	0.018(0.008)	0.034(0.008)
M17	0.054(0.010)	0.053(0.008)
G18.25+2.70	0.044(0.029)	0.016(0.015)
G18.60+2.40	0.030(0.010)	0.002(0.007)
G30.25−0.50	0.026(0.011)	0.043(0.012)

[7] Note that the equivalent eq. (6) of Heiles (1994) in incorrect.

which is generated over large ranges of Galactocentric radii and dominates the 11 cm continuum maps of Reich et al. (1990). We assume that the "diffuse component" presented in their Figures 53–57 is synchrotron radiation and that three fourths of its observed intensity is incident on the RRL-emitting region from behind; the brightness temperature of synchrotron radiation scales as $\nu^{-2.7}$. A typical diffuse-component 11 cm brightness temperature is ~ 3 K, so its contribution to T_B in equation (2) is ~ 13 K. We assume that the more structured "source component" in their maps is thermal radiation, which scales as ν^{-2}. For all of our positions except M17, W43, and S54, which are bright H II regions, the source component 11 cm brightness temperature is $\lesssim 1$ K, which contributes $\lesssim 4$ K to T_B. We add the 3 K cosmic background to these numbers to obtain a representative value $T_B \lesssim 20$ K.

For $T_B = 20$ K, we have the following: for Hα with $n \sim 167$, we have $f_{\rm NLTE} \sim 1.3$; for H243γ with $n_e = 10$, we have $f_{\rm NLTE} \sim 1.2$; and for H243γ with $n_e = 1$ cm^{-3}, we have $f_{\rm NLTE} \sim 2.1$. These are not always modest factors, and predict that the ratios of higher order lines to the α lines can be either considerably larger than or somewhat smaller than unity.

3.1.2. *Observational Indications*

The most convenient indicator of non-LTE effects is the intensity ratio of the higher order (i.e., $\Delta n > 1$) lines to the $\Delta n = 1$ line. The H243γ and H2667δ RRLs lie close to the H169α RRL, which we sometimes observed, but unfortunately these lines are located near 1350 MHz, which was often contaminated by interference. Nevertheless, we were able to obtain reasonably accurate ratios for a few sources.

Figure 3 shows the profiles, together with the fiducial marks and Gaussian fits for all three H RRLs and also the He169α and C169α RRLs. These profiles include only the 1350 MHz (169α) spectra, not the other Hα spectra at other frequencies, to ensure that all line intensities are calibrated identically. As in our other figures, the intensities are in units of the peak H169α line intensity. Figure 3 shows that we detected the H243γ line for four sources and the H267δ line for one source with enough S/N to fit Gaussians; in two additional sources, the H267δ line might be detected, but it is too close to the edge of the spectrum and the S/N is too poor to fit Gaussians. Table 2 shows the ratios of line intensities determined from the Gaussian fits, together with the LTE ratios (Menzel 1968).

For two positions, the H243γ/H169α ratio is comfortably close to LTE. G18.60+2.40 lies in the S54 worm, off any H II region, and the other is the H II region S54. S54 is a well-defined H II region with an obvious extended envelope. G18.60+2.40 represents the truly diffuse ELDWIM. Thus, we conclude that the RRL line intensities in the ELDWIM are close to the LTE values.

For W43, the observed H243γ/H169α ratio is smaller than LTE by a factor of about 2.5. We believe that this is the largest factor by which the ratio of a higher order transition to $\Delta n = 1$ RRL has ever been observed to depart from the LTE value. For W43, which is a small, dense H II region with emission measure EM $\sim 8 \times 10^5$ cm^{-6} pc, the smaller ratio is probably in accord with non-LTE calculations: at the 6 cm wavelength, Churchwell et al. (1978) find that H137β/H109α is within about 10% of the LTE value, which is consistent with Walmsley's (1980) curves showing that non-LTE effects should become important for $n \sim 100$–125,

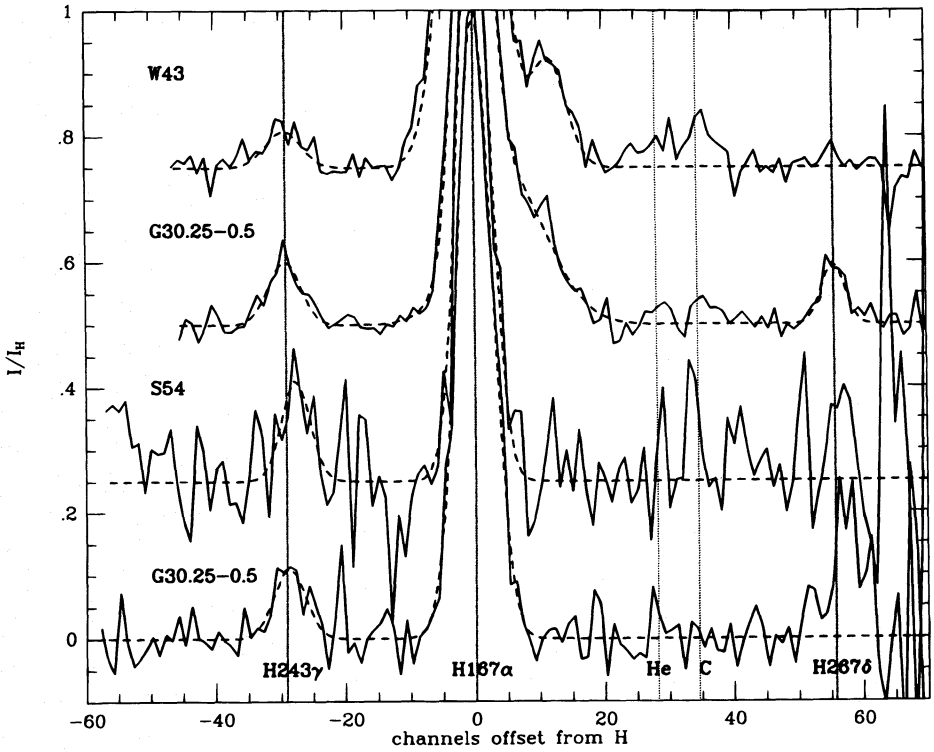

FIG. 3.—H169α and associated RRLs for NRAO data near 1350 MHz. For each spectrum, the intensity scale is in units of the intensity of the Gaussian fit to the H RRL as given in Table 1. The solid lines are the data. The dashed lines are the Gaussian fits to the spectra, which are summarized in Table 1. The vertical dotted lines are fiducial marks for the He169α, C169α, H243γ, and H267δ RRLs that would correspond to the H169α RRL if they had the same velocity.

depending on the degree of clumping. Walmsley calculates the expected line ratio for Orion and, from his Figure 6, one can deduce that factor of 2 departures from LTE in the sense that we observe for the H243γ/H169α ratio are not unreasonable.

For G30.25−0.50, the observed H243γ/H169α ratio is smaller than LTE by a factor of about 1.7. G30.25−0.50 does not lie near any cataloged H II region, so we cannot apply Walmsley's discussion. However, if our above estimates of the departure coefficients are correct, then it is difficult to understand such a deviation. We estimate that the 20 cm continuum temperature incident on G30.25−0.50 from behind is $\sim$20 K. This allows us to use our above estimates of $f_{\rm NLTE}$, namely, $f_{\rm NLTE} \sim 1.3$ for the Hα lines and, for the H243γ line, $f_{\rm NLTE} \sim 1.2$ and 2.1 for $n_e = 10$ and 1 cm^{-3}, respectively. The corresponding ratios are $f_{\rm NLTE,243\gamma}/f_{\rm NLTE,169\alpha} = 0.92$ and 1.62. These ratios cannot explain our observations, which require $f_{\rm NLTE,243\gamma}/f_{\rm NLTE,169\alpha} = 0.58$. Clearly, the stimulated emission effects for the H169α line must be significantly more important than indicated by extrapolation of existing theoretical results. To pursue this issue further would require theoretical models that apply to these low-density conditions where the background brightness temperature cannot be neglected.

We conclude that existing theoretical treatments of the departure coefficients and non-LTE RRL intensities cannot be applied in some cases for the ELDWIM. Fortunately, the conclusions of the present paper do not depend on the applicability of these results, because our main focus is on the He/H RRL ratio; non-LTE effects for the He and H lines should be identical except for the isotope shift, which is an exceedingly small perturbation for RRLs.

3.2. He/H *RRL Ratios for* H II *Regions*

Table 3 provides ratios of He/H integrated RRL intensities. If the He^+ and H^+ regions are coincident, then the line intensity ratio is simply equal to n_{He^+}/n_{H^+}. The nominal values of this ratio vary from 0 to 0.054.

The generally accepted cosmic abundance for He/H is very close to 0.10 (Boesgaard & Steigman 1985). Thus, our maximum He/H RRL ratio corresponds to $\chi_{He}/\chi_H = 0.54$. We generally consider the WIM to be fully ionized, with $\chi_H = 1$, and we shall assume this in the remainder of the discussion. Thus our maximum He/H RRL ratio corresponds to $\chi_{He} = 0.54$.

In H II regions the Galaxy-wide average $n_{He^+}/n_{H^+} = 0.074 \pm 0.003$, with no dependence on Galactocentric radius (Shaver et al. 1983). The smallness of this ratio as compared to the cosmic abundance ratio occurs because the He^+ zone in H II regions is smaller than the H^+ zone; when this correction is made, the H II region ratio is consistent with the generally accepted cosmic abundance (Osterbrock 1989).

For the individual H II regions S54, W43, and M17, we find $n_{He^+}/n_{H^+} = 0.053$, 0.018, and 0.054, respectively. These are much smaller ratios than the Galaxy-wide average of 0.074. They are also much smaller than higher frequency measurements, for which the ratios are $\lesssim$0.06, 0.082, and 0.096, respectively, at 14 GHz (McGee & Newton 1981; Shaver et al. 1983) and 0.071 and 0.090 for W43 and M17 at 8.6 GHz (Peimbert et al. 1992). Our low-frequency ratios are expected to be smaller because of the "geometric effect" (Mezger & Smith 1976): at low frequencies the high-density inner parts of H II regions are optically thick and the telescope beamwidths are large; thus, the data weight the outer, less dense parts of the H II region, where the He^+ zone has disappeared. For W43, this effect is evidently extreme; this may be related to the fact that S54 and M17 both have obvious extended envelopes, while W43 does not.

The same argument may well apply for G30.25−0.50, which is near the strong H II region G30.2−0.2 (Reifenstein et al. 1970), and to some extent for the average of $T_A > 100$ positions, whose relatively strong line intensities reflect their proximity to strong H II regions, as delineated above in § 2.1; the nominal He/H RRL ratios for these are 0.026 and 0.016, respectively.

3.3. He/H *RRL Ratios for the ELDWIM*

Our He/H RRL ratios for more diffuse regions are smaller. The regions include the positions G18.60+2.40, G18.25+2.70, S54 worm–S54, and $T_A < 100$; the ratios are 0.030 ± 0.010, 0.044 ± 0.029, -0.004 ± 0.013, and 0.000 ± 0.011, respectively.

Here and below we focus on the ratios for S54 worm–S54 and the $T_A < 100$ average. These are representative of truly diffuse regions. S54 worm–S54 samples many positions in the S54 worm but includes no standard H II region. $T_A < 100$ is most representative of the pervasive, diffuse ELDWIM, because it is an average of 138 positions. For purposes of discussion, we adopt the upper limit $n_{He^+}/n_{H^+} = 0.013$, which is the average of the 1 σ errors for these two averages. This corresponds to $\chi_{He} < 0.13$. To achieve such a low ratio in a standard H II region requires that the temperature of the ionizing star $T_* \lesssim 35{,}000$ K (equivalent to an O7 star; see Osterbrock 1989). Employing current knowledge about the initial mass function and the total Galactic star formation rate, it is difficult to simultaneously obtain such a "cool" ionizing spectrum together with the total Galactic ionization requirement for the WIM and H II regions. We refer to this as the *ionizing-spectrum problem*. The discussion of this problem is extensive, and we defer it to § 5 below.

3.4. *Obscure Observational Implications*

The low He^+ abundance in the ELDWIM has two curious, though obscure, observational implications. First, if χ_{He} were as large as χ_H, then the 8.7 GHz hyperfine line of $^3He^+$ would be detectable from the ELDWIM. The total electron column to the far side of the solar circle at $l = 0°$ is about 2×10^{21} cm^{-2} (Taylor & Cordes 1993), and a representative abundance is $^3He^+/H \sim 2 \times 10^{-5}$ (Balser et al. 1994). With full ionization of He, this would provide $\int T_B\, dv \sim 0.11$ K km s^{-1} for the $^3He^+$ line; the velocity width would be $\sim$30 km s^{-1} toward $l = 0°$, providing a line temperature of $\sim$4 mK. This is comparable to the intensity in the first detections of the line (Rood, Bania, & Wilson 1984). However, in fact χ_{He} is not large, and the $^3He^+$ line should not be (and apparently is not) detectable—it is at least 5–10 times weaker than the above estimate.

Second, Heiles (1994) has argued that the most important production agent for the global C^+ 158 μm radiation from the Galactic interior is the ELDWIM. This argument requires the primary ionization state of carbon to be C^+. The ionization potential of C^+ is 24.4 eV, just 0.2 eV less than that of He. The fact that He is mainly neutral in the ELDWIM is consistent with C being mainly C^+. The only

way to violate this consistency, i.e., for C^{++} to be the primary ionization state in the ELDWIM, is for the photoionizing spectrum to cut off sharply just above 24.4 eV. This is unlikely unless photoionization of He^+ is itself responsible for removing photon energies greater than 24.6 eV. We cannot assess the certainty of this in the absence of further information, but if the ionizing photons are produced by a continuous IMF of massive stars, as discussed in § 5.2 below, then there should be no sharp cutoff; the corollary is that C^+ should indeed be the dominant ionization species of carbon in the ELDWIM.

4. THE C RRLs

4.1. *The C RRLs a Tracer of Cold, Dense Gas*

The ratios of C/H integrated RRL intensities range between zero and 0.053. If the C and H RRLs are produced in the same region, then the line intensity ratio is simply equal to n_{C^+}/n_{H^+}. Some observed intensity ratios vastly exceed the cosmic abundance ratio C/H, which is about $4 \times 10^{-4}\delta$ (Spitzer 1978), where $\delta(\leq 1)$ accounts for the depletion of C onto dust grains. Clearly, the C RRL must come from a region in which H is predominantly neutral.

We expect the CRRL emission to arise in the cold, dense region that abuts an H II region; such environments are known as photodissociation regions (PDRs) (e.g., Hollenbach, Takahashi, & Tielens 1991, hereafter HTT). The electrons come exclusively from the C^+. Carbon is almost fully ionized, so that $n_e = n_{C^+} = 4 \times 10^{-4}\delta n_H$. Then, parameterizing in terms of the pressure $P_4 \equiv P/10^4 k = nT_4$ cm^{-3} K (where k is Boltzmann's constant), we have

$$\int T_{B,C}\, dv = f_{NLTE}\, 4.7 \times 10^{-3} v_9^{-1} \left(\frac{\delta}{0.5}\right)^2 T_2^{-5/2} P_4 N_{HTT} . \quad (3)$$

Here we have written the variables in terms of their approximate expected values for a PDR: T_2 is in units of 100 K, the carbon depletion δ is in units of its typical interstellar value ~ 0.5, and the H nuclei column density N_{HTT} is in terms of the value that characterizes the C^+-containing part of a PDR according to HTT ($N_{HTT} = N_H/5.9 \times 10^{21}$ cm^{-2}).

Assume for now that $f_{NLTE} = 1$, i.e., that stimulated emission is unimportant. We consider a "representative" observed value for the integral of the C RRL of 0.6 K km s^{-1} (the values range from 0.09 to 3.5 K km s^{-1}, so no value can be truly representative). This value requires $P_4 \approx 180$. With $T_2 = 1$ this means $n_H \approx 1.8 \times 10^4$ cm^{-3}, which is 18 times the density of HTT's "standard model," and with all C being singly ionized we have $n_e \approx 3.6$ cm^{-3}. We note that this value depends sensitively on the temperature; a factor of 2.5 smaller temperature lowers P_4 by a factor of 10.

Under these conditions, stimulated emission can be important for the C RRL. Dupree (1972) calculated departure coefficients for the low-temperature, low-n_e case. For the C166α RRL and $T_e = 10$–100 K, $(d \ln b_n)/dn$ is nearly a maximum as a function of n_e for $n_e = 0.1$–1 cm^{-3} and $b_n \sim 0.25$ and varies slowly with n_e, so we can be reasonably confident that we are not underestimating the stimulated emission. For $n_e = 1$ cm^{-3}, Dupree (1972) finds $(d \ln b_n)/dn \sim 0.01$ for $T = 20$–100 K. For $T_e \gtrsim 50$ K, Dupree's results must be corrected for the enhanced recombination rate resulting from dielectronic recombination involving the fine-structure ground-state transition of C (the excitation temperature of which is 92 K). This decreases $(d \ln b_n)/dn$ by a factor ~ 2, but increases b_n somewhat (Walmsley & Watson 1982); we ignore these corrections for the present crude level of approximation. We adopt $(d \ln b_n)/dn = 0.01$ and $b_n = 0.2$; this gives $f_{NLTE} = 0.2(1 + 0.15T_B)$.

We clearly detected the C RRL in the NRAO data for four positions: S54, G30.25−0.50, W43, and M17, with integrated intensities 86, 140, 780, and 3500 mK km s^{-1}, respectively. We observed continuum antenna temperatures for these positions of approximately 26, 19, 59, and 175 K, respectively[8]; (the antenna temperature is proportional to the brightness temperature integrated over the telescope beam). The C RRL strength tends to increase with continuum antenna temperature, which suggests that stimulated emission is indeed important for these positions. For W43, with a brightness temperature of ~ 50 K, it should make the line ~ 2 times stronger. This reduces the required value of P_4 and also, of course, the corresponding volume density of both H nuclei and electrons.

The C RRL was possibly detected in some of the HCRO spectra, but in no case is the line center correctly placed with respect to the H RRL, and all of the "detections" look suspicious. The continuum brightness temperatures for all of these positions are small, which is consistent with either the absence or the weakness of the C RRL in these data.

Our conclusions concerning the C RRL are consistent with earlier work as summarized, for example, by Dupree (1974), Pankonin (1980), Brown, Lockman, & Knapp (1978), Roelfsema (1990), and Roelfsema & Goss (1992), but with some differences. These summaries refer to bright, small ($\lesssim 1$ pc), and well-defined H II regions. Although W43, M17, and S54 are all reasonably well defined on the maps of Reich et al. (1990), not all of them are small: S54 is comparable to or larger than our telescope beam (HPBW = 21′), and the large distance (~ 3 kpc; Reifenstein et al. 1970) means that our observations sample an 18 pc size region. Our other C RRL position, G30.25−0.50, lies on a large ($\gtrsim 1°$) continuum plateau, and little of the integrated intensity is contributed by small regions. These two regions cannot be classified as small H II regions, and, with the correction for stimulated emission, our estimated volume densities in the PDR are smaller. However, the same physical processes are at work.

4.2. *The C RRLs and the* C^+ 158 μm *Line toward W43*

Toward H II regions the data are consistent with both lines tracing PDRs. We consider the relationship between the C RRL and the C^+ 158 μm line, under the assumption that the two lines are produced in the same region. As discussed above, the C RRLs are produced in dense, neutral PDRs. In such regions collisional excitation of the 158 μm line occurs primarily from neutral H atoms and molecules. The critical density for these neutral collisions is ~ 3000 cm^{-3} (Hollenbach & McKee 1989), which is less than or approximately equal to the volume densities we estimate

[8] The zero points of these antenna temperatures are very uncertain because the antenna temperatures are derived from the measured system temperatures averaged over the integration. These system temperatures are not very accurately measured and also include the sidelobe pickup of the Earth's thermal radiation; we neglected these problems and adopted the measured continuum antenna temperatures as the system temperatures minus 23 K, which is the approximate system temperature on "cold sky."

above. Thus, to ease the discussion, we assume that the 158 μm levels are in collisional equilibrium, and obtain

$$I_{C^+,-4} = \frac{27.3(\delta/0.5)N_{HTT}}{1 + e^{0.92/T_2}/2}, \quad (4)$$

where $I_{C^+,-4}$ is the integrated intensity of the 158 μm line in units of 10^{-4} ergs cm^{-2} s^{-1} sr^{-1}.

Shibai et al. (1991) scanned across the H II region W43 and found a peak $I_{C^+,-4} \sim 7$; this can be compared directly to our observation of W43, for which $\int T_{B,C}\, dv \sim 0.78$ K km s^{-1}. With our above estimate $f_{NLTE} \sim 2$ for W43 and assuming $T_2 = 1$, this yields $P_4 \sim 200$ and $N_{HTT} \sim 0.6$.

This corresponds quite well with the PDR interpretation. In a PDR, and in the absence of a magnetic field, the gas pressure should be comparable to the gas pressure in the adjacent ionized gas. With $P_4 \sim 200$ and $T_e = 10^4$ K we expect $n_e \sim 100$ cm^{-3}. Given the uncertainties, this is not too inconsistent with the mean electron density in the H II region W43, which is measured to be about $n_e \sim 150$ cm^{-3} (Reifenstein et al. 1970). Their value was derived from 5 GHz observations and refers to a smaller region than that sampled by our telescope beam, which may account for the different values of n_e.

5. DISCUSSION OF THE He^+/H^+ RATIO

In this section we return to the He^+/H^+ ratio and consider three explanations for its low value. We begin with a discussion of related observational constraints in § 5.1. Section 5.2 considers the conventional ionization mechanism, photoionization of the ELDWIM by stars that populate a standard IMF with a reasonable upper mass cutoff. Sections 5.3 and 5.4 consider less conventional mechanisms, one involving an excess output of ionizing photons observed from B stars and one invoking production of ionizing photons by decay of dark matter.

5.1. *Observational Constraints*

First we recall the information on the ionizing spectrum of the ELDWIM: the spectrum is *soft* in the sense that χ_{He}/χ_H is $\lesssim 0.27$ locally and $\lesssim 0.13$ globally (Reynolds & Tufte 1995; § 3.3 above). This implies that the ratio of the He ionizing photon production rate $Q(He^0)$ to $Q(H^0)$ is $\lesssim 0.013$–0.027. This is the ionizing-spectrum problem as defined above.

Next, consider the global ionization requirements in the Galaxy. Mezger (1978) has made a detailed estimate of these requirements. He assumed the then standard solar Galactocentric radius $R_{gal,\odot} = 10$ kpc, and his results must be corrected to the currently accepted value $R_{gal,\odot} = 8.5$ kpc. This correction multiplies all lengths by 0.85, the volume emissivity by 1/0.85, and the deduced number of ionizing photons by 0.85^2. Furthermore, he used radio continuum data to model the H recombination rate out to $R_{gal}/R_{gal,\odot} \sim 1.3$, but for $R_{gal}/R_{gal,\odot} \gtrsim 0.8$ (which corresponds to $l \gtrsim 50°$) his results depend sensitively on the observed intensities, which are weak. We do not trust his results for $R_{gal}/R_{gal,\odot} \gtrsim 0.8$; our distrust is manifest for $R_{gal}/R_{gal,\odot} = 1$, where Reynolds (1991) derives $\langle n_e^2 \rangle = 0.0066$ cm^{-6} at $z = 0$, while Mezger's (1978) model predicts $\langle n_e^2 \rangle = 0.04$ cm^{-6}. Reynolds' results indicate that the global contribution to the total Galactic recombination rate from $R_{gal}/R_{gal,\odot} \gtrsim 1$ is small. Accordingly, we accept Mezger's results for $R_{gal}/R_{gal,\odot} \leq 0.8$ and adopt a recombination rate of 0 for $R_{gal}/R_{gal,\odot} > 0.8$. Note that the ELDWIM absorbs most of these photons, ~85% according to Mezger. With these corrections, we obtain a total Galactic ionizing photon production rate $S_{53} = 1.4$ (S_{53} is the H ionizing photon production rate in units of 10^{53} s^{-1}).[9]

Before beginning, we remind the reader of the important distinguishing characteristic of the ELDWIM: the ELDWIM is pervasive and widely distributed. In contrast, hot stars are usually considered to produce locally confined H II regions. This leads to the *morphological problem*: if stars produce the photons that ionize the ELDWIM, how do the photons travel long distances? This problem can be explained in at least two conventional ways. One involves a clumpy medium in which the WIM has a roughly uniform low-density component with higher density clumps interspersed (Miller & Cox 1993). The other invokes clusters of massive stars together with successive generations of star formation: supernovae in the older generations of a star cluster blow a huge supershell, or "worm." the interior of which contains the hot ionized medium, and hot stars in successive generations of the same cluster produce ionizing photons that can travel freely to the distant worm walls, which become fully ionized with low emission measures (the "worm-ionized medium"; Heiles 1992, 1993a, b; HRK). If the ELDWIM is photoionized by hot stars that are members of a standard IMF, then one or both of these two situations must exist to account for the morphological problem.

5.2. *Explanation in Terms of a Conventional IMF with Upper Mass Limit M_u*

This section discusses the following questions: (1) If the ELDWIM is ionized by OB stars with a composite spectrum that is "cool" enough to account for our low He/H ratio, and if these stars exist in accordance with the currently accepted IMF with upper mass cutoff M_u, what is the *upper* limit on M_u? (2) If the global Galactic star formation rate is the currently accepted value, and if these stars exist in accordance with the currently accepted IMF with upper mass cutoff M_u and produce the total observed Galactic ionization rate, what is the *lower* limit on M_u? (3) Are these lower and upper limits compatible?

5.2.1. *Formulation*

We now consider the following question: if this soft spectrum is provided by OB stars with masses between $M_l \simeq 8\ M_\odot$ and M_u, what is the upper limit on M_u? Define $f_*(m)dm \equiv$ fraction of stars with masses between m and $m + dm$, $\bar{s}_H(m) \equiv$ mean H ionizing photon luminosity of star with mass m, and $\bar{s}_{He}(m) \equiv$ mean He ionizing photon luminosity of star with mass m, where $\bar{s}_H(m)$ and $\bar{s}_{He}(m)$ are the means over the main-sequence lifetimes of stars. Then, if the star formation rate is $\dot{N}_*$, $Q(H^0)$ and $Q(He^0)$ are given by

$$Q(H^0) = \dot{N}_* \int_{M_l}^{M_u} \bar{s}_H(m)\tau_{MS}(m) f_*(m) dm \quad (5a)$$

[9] This is about half the estimate of Bennett et al. (1994), whose paper came to our attention only after our paper was written. If their higher number is correct, then the lower limit on M_u that we derive below must be raised even higher than 73 $M_\odot$, making the discrepancy that we derive even harder to reconcile.

and

$$Q(\mathrm{He}^0) = \dot{N}_* \int_{M_l}^{M_u} \zeta(m)\bar{s}_{\mathrm{H}}(m)\tau_{\mathrm{MS}}(m) f_*(m) dm \ , \quad (5b)$$

where $\tau_{\mathrm{MS}}(m)$ is the main-sequence lifetime of a star with mass m, and

$$\zeta(m) \equiv \bar{s}_{\mathrm{He}}/\bar{s}_{\mathrm{H}} \ . \quad (5c)$$

We need to determine the $\dot{N}_*$ and M_u that satisfy the observed properties and are also consistent with other observations. Since it is the massive stars that provide ionizing photons, $Q(\mathrm{H}^0)$ and $Q(\mathrm{He}^0)$ are not sensitive to the lower limit M_l and we take $M_l = 8\ M_\odot$.

We first consider $\tau_{\mathrm{MS}}(m)$, $\bar{s}_{\mathrm{H}}(m)$, and $\zeta(m)$. In principle, one can derive these stellar properties self-consistently from models of stellar evolution and stellar atmosphere, which is beyond the scope of this paper. Instead, we simply use the published results on these parameters:

1. $\tau_{\mathrm{MS}}(m)$.—We adopt the main-sequence lifetime $\tau_{\mathrm{MS}}(m)$ (yr) of Güsten & Mezger (1982, hereafter GM), which is given by

$$\tau_{\mathrm{MS}}(m) = 1.2 \times 10^9 m^{-1.85} + 3 \times 10^6 \ , \quad \text{for } 8\ M_\odot \lesssim m \lesssim 60\ M_\odot \ . \quad (6)$$

The main-sequence lifetime in equation (6) is based on various stellar evolutionary models with $Z = 0.02$–0.03 and neglects the mass loss. The effect of mass loss on the main-sequence evolution, however, is small (Maeder 1991). The parameter τ_{MS} in equation (6) agrees with the results of recent model calculations by Schaller et al. (1992), with $Z = 0.02$, within 10% between $m = 8$ and 60 $M_\odot$. For larger masses, the extrapolation of equation (6) yields a larger discrepancy, e.g., 18% at $m = 85\ M_\odot$.

2. $\bar{s}_{\mathrm{H}}(m)$.—We adopt $\bar{s}_{\mathrm{H}}(m)$ (photons s^{-1}) of GM. A convenient numerical approximation is (Cox, Krügel, & Mezger 1986)

$$\log \bar{s}_{\mathrm{H}} = 38.3 + 8.16 \log m - 0.24 \log^2 m - 0.41 \log^3 m \ . \quad (7)$$

The parameter $\bar{s}_{\mathrm{H}}(m)$ is computed along evolutionary tracks using stellar evolutionary and atmospheric models. GM used the same evolutionary models that they used in deriving the main-sequence lifetime in equation (6) and the LTE line-blanketed models of Kurucz (1979). In addition to the uncertainties associated with evolutionary models, which appear to be small, there are at least two sources of errors. First, there is an uncertainty associated with stellar atmospheric models in computing Lyman continuum (Lyc) photon fluxes for given T_{eff} and $\log g$. This again appears to be small. Vacca, Garmany, & Shull (1995, hereafter VGS) recently compared the Lyc photon fluxes predicted from various atmospheric models and concluded that they are consistent within 20%. The second source of uncertainty originates from the discrepancy between the effective temperature and gravity of atmospheric models, $T_{\mathrm{eff},A}$ and $\log g_A$, and those of evolutionary models, $T_{\mathrm{eff},E}$ and $\log g_E$.

For a given luminosity per unit mass at some particular evolutionary stage, one can determine $T_{\mathrm{eff},A}$ and $\log g_A$ using stellar atmospheric models. The important point is that they differ from $T_{\mathrm{eff},E}$ and $\log g_E$ considerably for high-mass stars (VGS). (Alternatively, one can say that, for a given T_{eff} and gravity, the luminosity per unit mass predicted from atmospheric models differs from that predicted from evolutionary models. VGS called this the "mass discrepancy.") According to Table 5 of VGS, $T_{\mathrm{eff},A}$ is greater than $T_{\mathrm{eff},E}$ by 4% and 12% for $m \cong 19.4$ and 41 $M_\odot$, which in turn results in 74% and 82% increases of Lyc photon fluxes, respectively. Because of the difference in gravity, the differences in $\bar{s}_{\mathrm{H}}(m)$ are even larger: factors of 1.8 and 2.4 for $m = 19.4\ M_\odot$ and 41 $M_\odot$, respectively. Hence, if the effective temperature and gravity corresponding to m are close to $T_{\mathrm{eff},A}$ and $\log g_A$ instead of $T_{\mathrm{eff},E}$ and $\log g_E$, then the $\bar{s}_{\mathrm{H}}(m)$ would be considerably larger than that of equation (7). However, according to VGS, the discrepancy is most likely due to the simplifying assumptions in stellar atmospheric models, e.g., plane-parallel and hydrostatic atmosphere. For this reason, we use the evolutionary models and their adaptation in the form of equation (7).

3. $\zeta(m)$.—In order to compute $\zeta(m)$, we need the *time-averaged* He ionizing photon luminosity $\bar{s}_{\mathrm{He}}(m)$, which is not available in the literature as far as we are aware. Instead we use the relation between ζ and T_{eff} obtained for the characteristic parameters of main-sequence stars. Since the characteristic parameters of main-sequence stars represent the average values, we may consider them to be close to the time-averaged parameters, although the samples in the two averages are not the same. We convert T_{eff} to m using the relation between T_{eff} and the (evolutionary) mass in Table 5 of VGS.

Values of ζ predicted from stellar atmospheric models are rather uncertain. For example, VGS found that their ζ's computed from the LTE line-blanketed models of Kurucz (1992) are roughly a factor of 2 smaller than those determined from the non-LTE models. As we will see in § 5.2.3, our results are not affected much by this factor of 2 uncertainty. In this paper, we adopt ζ's determined from the non-LTE models of Kudritzki et al. (1991) without wind blanketing, the effect of which is negligible. A convenient numerical expression is

$$\log \zeta(m) = \begin{cases} -33.48 + 40.8 \log m - 12.63 \log^2 m & \text{for } m \le 40\ M_\odot \ , \\ -1.63 + 0.95 \log m - 0.172 \log^2 m & \text{for } m \ge 40\ M_\odot \ . \end{cases} \quad (8)$$

The above numerical expression is obtained from those data with $23\ M_\odot < m < 88\ M_\odot$ and therefore $\zeta(m)$ outside this mass range is uncertain.

4. $f_*(m)$.—We adopt McKee's (1989) expression for the Scalo (1986) IMF:

$$f_*(m) = 0.063 C_f m^{-2.5} \quad \text{for } m > 8\ M_\odot \ , \quad (9)$$

where C_f is a numerical factor describing the uncertainty. By comparing with the local stellar surface density and the local pulsar birthrate, McKee concluded $C_f = 1$–2. Note that the IMF in equation (9) is not self-consistent with our adopted stellar parameters. For example, the main-sequence lifetimes used by Scalo (1986) are systematically longer than those in equation (6) by a factor of 1.3–1.6 for $m = 8$–$60\ M_\odot$.

5.2.2. *Results*

Table 4 summarizes the results obtained by using the above stellar properties. Column (1) is M_u in $M_\odot$. Columns (2)–(4) represent τ_{MS}, $\bar{s}_{\mathrm{H}}$, and ζ for $m = M_u$; they are listed to show how the stellar parameters vary with m. Column (5) is

TABLE 4

IONIZING PARAMETERS FOR A GIVEN UPPER-MASS LIMIT M_u

M_u ($M_\odot$) (1)	$\tau_{MS}(m)$ (10^6 yr) (2)	$\bar{s}_H(m)$ (10^{49} s^{-1}) (3)	$\zeta(m)$ (4)	$Q(H^0)/\dot{M}_*$ (10^{50} s^{-1} $M_\odot^{-1}$ yr) (5)	$\dot{M}_*$[a] ($M_\odot$ yr^{-1}) (6)	$Q(He^0)/Q(H^0)$ (7)
10.5.....	0.19E+02	0.88E−03	0.10E−04	0.10E+01	0.13E+04	0.30E−05
12.3.....	0.14E+02	0.24E−02	0.10E−03	0.23E+01	0.60E+03	0.26E−04
14.5.....	0.12E+02	0.65E−02	0.75E−03	0.44E+01	0.31E+03	0.18E−03
17.1.....	0.93E+01	0.17E−01	0.42E−02	0.80E+01	0.18E+03	0.11E−02
20.1.....	0.77E+01	0.41E−01	0.17E−01	0.14E+02	0.10E+03	0.48E−02
22.4.....	0.68E+01	0.74E−01	0.38E−01	0.19E+02	0.73E+02	0.11E−01
24.3.....	0.63E+01	0.11E−00	0.63E−01	0.25E+02	0.57E+02	0.20E−01
26.3.....	0.58E+01	0.17E−00	0.98E−01	0.31E+02	0.45E+02	0.33E−01
28.6.....	0.54E+01	0.25E−00	0.14E−00	0.39E+02	0.36E+02	0.51E−01
31.0.....	0.51E+01	0.38E−00	0.19E−00	0.49E+02	0.28E+02	0.74E−01
33.6.....	0.48E+01	0.55E−00	0.23E−00	0.62E+02	0.23E+02	0.10E−00
38.5.....	0.44E+01	0.10E−01	0.29E−00	0.88E+02	0.16E+02	0.15E−00
45.3.....	0.40E+01	0.20E−01	0.30E−00	0.13E+03	0.11E+02	0.20E−00
53.3.....	0.38E+01	0.37E−01	0.31E−00	0.19E+03	0.72E+01	0.23E−00
62.6.....	0.36E+01	0.64E−01	0.33E−00	0.28E+03	0.51E+01	0.26E−00
73.7.....	0.34E+01	0.11E−02	0.35E−00	0.38E+03	0.37E+01	0.28E−00
86.7.....	0.33E+01	0.17E−02	0.37E−00	0.51E+03	0.28E+01	0.30E−00
102.0.....	0.32E+01	0.25E−02	0.38E−00	0.66E+03	0.21E+01	0.32E−00

[a] $\dot{M}_*$ is the star formation rate required to obtain $Q(H^0) = 1.4 \times 10^{53}$ s^{-1}.

$Q(H^0)$ normalized by the star formation rate $\dot{M}_*(M_\odot\ \mathrm{yr}^{-1})$, integrated over mass as in equation (5a). We converted $\dot{N}_*$ in equation (5) using $\dot{M}_* = \dot{N}_*/\bar{m}_*$, where $\bar{m}_* = 0.51\ M_\odot$ is the mean mass of stars (Scalo 1986). Column (6) is the star formation rate necessary for stars having $m \le M_u$ to produce $Q(H^0) = 1.4 \times 10^{53}$ photons s^{-1}. Column (7) is $Q(He^0)/Q(H^0)$.

5.2.3. *Discussion and Conclusions*

According to Table 4 and the observational constraint discussed in § 5.1, the ionization spectrum requires the *upper limit* $M_u \lesssim 26\ M_\odot$. This corresponds to a total Galactic star formation rate of $\sim 50\ M_\odot\ \mathrm{yr}^{-1}$. This is far higher than estimates of the Galactic star formation rate based on other observations, which lie in the range 1.8–3.6 $M_\odot\ \mathrm{yr}^{-1}$ (McKee 1989). From Table 4, McKee's higher rate of 3.6 $M_\odot\ \mathrm{yr}^{-1}$ requires the *lower limit* $M_u \gtrsim 73\ M_\odot$. The discrepancy between these upper and lower limits on M_u is unacceptably large.

The discrepancy is reduced, but not much, if we consider the uncertainties in various stellar parameters. First, note that even if values of $\zeta(m)$ are smaller than those in Table 4 by a factor of 2 as predicted from the LTE line-blanketed model atmospheres (see § 5.2.1), the upper limit on M_u increases only a little, to 29 $M_\odot$. Also, in equation (8) $\zeta(m)$ increases rapidly near 23 $M_\odot$, which means that the uncertainty in $\zeta(m)$ affects the upper limit on M_u very little. Second, if the values of $\bar{s}_H(m)$ are greater than those in Table 4 by a factor of 2 because of the VGS mass discrepancy (see § 5.2.1), then the lower limit decreases to 53 $M_\odot$—but in this case the upper limit also decreases, because the effective temperature for a given mass stellar increases. Clearly, a detailed, self-consistent study needs to be done. Nevertheless, our results show that the level of discrepancy is not easily compromised by the uncertainties in stellar parameters and in the total Galactic production of UV photons.

One can further ease the situation by hypothesizing that the stars earlier than O7 are selectively hidden inside dense clouds, where they produce classical H II regions whose He^+ zones are confined by the cloud. This is an extreme form of the geometric effect mentioned above in § 3.2. It is consistent with the "worm-ionized medium" picture as long as the most massive newly formed stars reside in dense H II regions that are small enough to be density-bounded but large enough to confine the He^+ zone. Such a condition might not be unreasonable, and its consequence needs to be explored.

If the discrepancy is in fact real, then it has implications for all of the factors entering the above discussion—or it means that another source of ionization exists. We now consider two such possibilities.

5.3. *Excess Ionizing Photons from B Stars*

One unconventional explanation for the ionizing-spectrum problem involves excess, unpredicted ionizing radiation from stars. Cassinelli et al. (1995) find that the B2 II star ϵ CMa emits 30 times more H ionizing photons than expected from model atmosphere calculations. If such excesses are common among B stars, then both the morphological and the ionization difficulties might be solved. Such stars are reasonably pervasively distributed, and the ratio of H ionizing to He ionizing photons is large. Unfortunately, the observational sample is limited to a single star, so we do not know how common the ionizing-photon excess is in B stars. In the absence of further information we cannot realistically assess the viability of this explanation.

5.4. *Ionizing Photons from the Decay of Dark Matter*

Sciama (1990) has put forth a significantly more unconventional explanation which involves the production of photons by the decay of dark matter. If these photons have energy greater than 13.6 eV (the ionization potential of H) and less than 24.6 eV (the ionization potential of He), then they would act as a distributed source of ionization that satisfies both the morphological and the ionizing-spectrum problems. Sciama derives a photon energy of ~ 14 eV from other observational constraints, which of course also satisfies our requirements.

While this hypothesis explains both the morphological and the ionizing-spectrum problems, it is not powerful enough to account for the observed intensity of the emis-

sion. Sciama explicitly predicts the recombination rate versus Galactocentric radius: the density of dark matter varies as $2/[1 + (R_{gal}/R_{gal,\odot})^2]$ (or, alternatively, as $4/(1 + R_{gal}/R_{gal,\odot})^2$. The rate of production of ionizing photons is proportional to the density of dark matter, and as long as the H I is opaque to the 14 eV photons—which occurs at very low column densities—then the recombination rate, and with it the radio continuum and RRL volume emissivities, is also proportional to the density of dark matter. For the range of R_{gal} in which the ELDWIM produces observable RRLs, about 4–7 kpc, Sciama predicts $\langle n_e \rangle$ close to the value deduced from pulsars and $\langle n_e^2 \rangle \sim 0.06$ cm^{-6}. However, the observed (or rather, deduced) value of $\langle n_e^2 \rangle$, from the volume emissivity of thermal radio continuum radiation, is roughly an order of magnitude larger. Specifically, Mezger (1978) finds that $\langle n_e^2 \rangle \sim 0.61$ cm^{-6} for the annulus $R_{gal} \approx 3.8 \pm 0.4$ kpc (Here we have scaled his results as described in § 5.1).

Sciama's mechanism also fails to account for the z extent of our observed RRLs. The z extent of the putative dark matter is much larger than that of the neutral gas, so the predicted ionizing photon production rate is independent of z within the neutral gas layer. This would produce thermal radio continuum and RRL intensities that are independent of z up to the height where the ionizing photons can escape the neutral gas layer. However, the observed intensities fall off much faster with z. This is simply another illustration of the fact that Sciama's photon production rate is insufficient to account for total Galactic ionization requirement, as discussed in the above paragraph.

We conclude that Sciama's dark matter decay cannot account for our observed RRLs. Of course, the corollary is that neither can it account for our anomalously low He/H RRL intensity ratio. We note emphatically that this does not mean that Sciama's hypothesis is incorrect, only that it does not apply to our results.

6. SUMMARY

We have observed radio recombination lines at ~ 1.4 GHz toward the Galactic interior at hundreds of positions (Heiles et al. 1995). In some cases the S/N in good enough for us to observe not only the Hα but also the Hγ, Hδ, Heα, and Cα RRLs.

The ratio $\chi_{He}/\chi_H \equiv (n_{He^+}/n_{He})/(n_{H^+}/n_H)$ varies from being undetectable at the $\sim 10\%$ level (for data with weaker H RRLs, which sample the diffusely distributed ELDWIM) to 0.54 (for the strong H II region M17). All ratios are lower than the cosmic abundance of He/H. For the H II regions, the low ratios are interpretable in terms of the "geometric effect" (Mezger & Smith 1976), which involves the noncoincidence of the He^+ and H^+ zones and the radio optical depths of H II regions.

However, for the ELDWIM, the low values of χ_{He}/χ_H are more difficult to explain because of three problems: the "morphological problem," which is the question of how diffusely distributed ionized gas can exist in the interstellar medium if the source of ionizing photons is hot stars; the "ionizing-spectrum problem," which is the question of how photons with energy greater than 24.6 eV can be systematically excluded from the ELDWIM; and the total Galactic ionization requirement, which is combination with the ionizing-spectrum problem cannot easily be satisfied by stars and a conventional IMF. In § 5.2.3 we concluded that the ionizing-spectrum problem requires an upper mass limit for the IMF $M_u < 26\ M_\odot$, while the total Galactic ionization requirement requires $M_u > 73\ M_\odot$. These limits are not very accurate because of uncertainties in stellar parameters and the total Galactic UV photon production rate. Nevertheless, the discrepancy between the upper and lower limits on M_u is substantial and cannot easily be rationalized.

It is conceivable that the resolution of the discrepancy lies simply in our having underestimated the uncertainties in the various parameters of the IMF, stellar parameters, the Galactic ionization rate, and the Galactic star formation rate. Also, we might hypothesize that stars earlier than O7 are selectively hidden inside dense clouds, where they produce classical H II regions whose He^+ zones are confined by the cloud. In any case, the discrepancy exposes our ignorance in these matters and underscores the need for a deeper understanding of these issues. If the situation cannot be understood in these terms, then a source of ionization other than conventionally understood starlight exists.

We considered two other sources of ionization in §§ 5.3 and 5.4. In one, many B stars might have EUV excesses, as found for the B2 star ϵ CMa (Cassinelli et al. 1995); unfortunately, not enough observational information is available on this point to make a definitive statement. In the other, diffusely distributed dark matter decays, producing H ionizing photons of energy ~ 14 eV (Sciama 1990); we showed that this mechanism is not sufficiently powerful to account for the enhanced recombination rate observed toward the Galactic interior.

We detect the C RRL toward H II regions. The physics of C RRLs toward H II regions has a long history and is well understood as arising from photodissociation regions. We compare the C RRL with the C^+ 158 μm line toward W43 and derive relatively unambiguous values for physical parameters in the associated photodissociation region; they are consistent with theoretical models of PDRs.

It is a pleasure to thank Joe Cassinelli, Ed Churchwell, John Mathis, Chris McKee, Ron Reynolds, Bill Watson, and especially Don Cox for helpful comments during the preparation of this manuscript. This work was supported in part by an NSF grant to C. H. B.-C. K. has been supported in part by the 1994 KOSEF International Cooperative Research Fund.

REFERENCES

Balser, D. S., Bania, T. M., Brockway, C. J., Rood R. T., & Wilson, T. L. 1994, ApJ, 430, 667
Bennett, C. L., et al. 1994, ApJ, 434, 587
Boesgaard, A. M., & Steigman, G. 1985, ARA&A, 23, 319
Brocklehurst, M. 1970, MNRAS, 148, 417
Brown, R. L., Lockman, F. J., & Knapp, G. R. 1978, ARA&A, 16, 445
Cassinelli, J. P., et al. 1995, ApJ, 438, 932
Cersosimo, J. C. 1990a, ApJ, 349, 67
———. 1990b, in Radio Recombination Lines: 25 Years of Investigation, ed. M. A. Gordon & R. L. Sorochenko (Dordrecht: Kluwer), 237
Churchwell, E., Smith, L. F., Mathis, J., Mezger, P. G., & Huchtmeier, W. 1978, A&A, 70, 719
Cooper, B. F. C. 1976, in Methods Exp. Phys., 12B, 280
Cox, P., Krügel, E., & Mezger, P. G. 1986, A&A, 155, 380
Domgörgen, H & Mathis, J. S. 1994, ApJ, 428, 647
Dupree, A. K. 1972, ApJ, 173, 293
———. 1974, ApJ, 187, 25
Goldberg, L. 1966, ApJ, 144, 1225
Güsten, R., & Mezger, P. G. 1982, Vistas Astron., 26, 159 (GM)
Heiles, C. 1989, ApJ, 336, 808

Heiles, C. 1992, in Evolution of Interstellar Matter and Dynamics of Galaxies, ed. J. Palouš, W. B. Burton, & P. O. Lindblad (Cambridge: Cambridge Univ. Press), 12
———. 1993a, in Reviews in Modern Astronomy 6: Stellar Evolution and Interstellar Matter, ed. G. Klare (Hamburg: Astronomische Gesellschaft), 19
———. 1993b, in Star Formation, Galaxies and the Interstellar Medium, ed. J. Franco, F. Ferrni, & G. Tenorio-Tagle (Cambridge: Cambridge Univ. Press), 245
———. 1994, ApJ, 436, 720
Heiles, C., Reach, W. T., & Koo, B.-C. 1995, ApJ, submitted (HRK)
Hollenbach, D. & McKee, C. F. 1989, ApJ, 342, 306
Hollenbach, D. J., Takahashi, T., & Tielens, A. G. G. M. 1991, ApJ, 377, 192 (HTT)
Koo, B.-C., Heiles, C., & Reach, W. T. 1992, ApJ, 390, 108
Kudritzki, R., Gabler, D., Kunze, A. W. A., & Pauldrach, J. 1991, in Massive Stars in Starbursts, ed. C. Leitherer, N. R. Walborn, T. M. Heckman, & C. A. Norman (Cambridge: Cambridge Univ. Press), 59
Kulkarni, S. R., & Heiles, C. 1987, in Interstellar Processes, ed. D. J. Hollenbach & H. A. Thronson, Jr. (Dordrecht: Reidel), 87
Kurucz, R. L. 1979, ApJS, 40 1
———. 1992, in IAU Symp. 149, The Stellar Populations of Galaxies, ed. B. Barbuy & A. Renzini (Dordrecht: Kluwer), 225
Lockman, F. J. 1976, ApJ, 209, 429
———. 1980, in Radio Recombination Lines, ed. P. A. Shaver, (Dordrecht: Reidel), 185
Mathis, J. S. 1986, ApJ, 301, 423
McGee, R. X., & Newton, L. M. 1981, MNRAS, 196, 889
McKee, C. F. 1989, ApJ, 345, 782
Maeder, A. 1991, in Massive Stars in Starbursts, ed. C. Leitherer, N. R. Walborn, T. M. Heckman, & C. A. Norman (Cambridge: Cambridge Univ. Press), 97
Menzel, D. H. 1968, Nature, 218, 756
Mezger, P. G. 1978, A&A, 70, 565
Mezger, P. G., & Smith, L. F. 1976, A&A, 47, 143
Miller, W. W. III, & Cox, D. P. 1993, ApJ, 417, 579
Müller, P., Reif, K., & Reich, W. 1987, A&A, 183, 327
Osterbrock, D. E. 1989, Astrophysics of Gaseous Nebulae and Active Galactic Nuclei (Mill Valley: Univ. Science Books), 24
Pankonin, V. 1980, in Radio Recombination Lines, ed. P. A. Shaver (Dordrecht: Reidel), 111
Petuchowski, S. J., & Bennett, C. L. 1993, ApJ, 405, 591
Peimbert, M., Rodríguez, L. F., Bania, T. M., Rood, R. T., & Wilson, T. L. 1992, ApJ, 395, 484
Reich, W., Fürst, E., Reich, P., & Reif, K. 1990, A&AS, 85, 633
Reifenstein, E. C., Wilson, T. L., Burke, B. F., Mezger, P. G., & Altenhoff, W. J. 1970, A&A, 4, 357
Reynolds, R. J. 1991, ApJ, 372, L17
Reynolds, R. J., & Tufte, S. L. 1995, ApJ, 439, L17
Roelfsema, P. R. 1990, in Radio Recombination Lines: 25 Years of Investigation, ed. M. A. Gordon & R. L. Sorochenko (Dordrecht: Kluwer), 259
Roelfsema, P. R., & Goss, W. M. 1992, A&A, Rev., 4, 161
Rood, R. T., Bania, T. M., & Wilson, T. L. 1984, ApJ, 280, 629
Scalo, J. M. 1986, Fundam. Cosmic Phys., 11, 1
Schaller, G., Schaerer, D., Meynet, G., & Maeder, A. 1992, A&AS, 96, 269
Sciama, D. W. 1990, ApJ, 364, 549
Sejnowski, T. J., & Hjellming, R. M. 1969, ApJ, 156, 915
Shaver, P. A., McGee, R. X., Newton, L. M., Danks, A. C., & Pottasch, S. R. 1983, MNRAS, 204, 53
Shibai, H., et al. ApJ, 374, 522
Spitzer, L. 1978, Physical Processes in the Interstellar Medium (New York: Wiley)
Taylor, J. H., & Cordes, J. M. 1993, ApJ, 411, 674
Vacca, W. D., Garmany, C. D., & Shull, J. M. 1995, ApJ, preprint (VGS)
Walmsley, C. M. 1980, in Radio Recombination Lines, ed. P. A. Shaver (Dordrecht: Reidel), 37
Walmsley, C. M., & Watson, W. D. 1982, ApJ, 260, 317